SJMI(2020) 01; 43-61

ISSN : 2635-4608

DOI http://dx.doi.org/10.31916/sjmi2020-01-05

Analysis of Fitting Degree of MRI and PET Images in Simultaneous MR-PET Images by Machine Learning Neural Networks

[1]*GilJae Lee*, [1†] *Hwunjae Lee*, [2*]*Gyehwan Jin*

Received: 27 August 2020 / Accepted: 22 November 2020 / Published online: 28 December 2020

Abstract Simultaneous MR-PET imaging is a fusion of MRI using various parameters and PET images using various nuclides. In this paper, we performed analysis on the fitting degree between MRI and simultaneous MR-PET images and between PET and simultaneous MR-PET images. For the fitness analysis by neural network learning, feature parameters of experimental images were extracted by discrete wavelet transform (DWT), and the extracted parameters were used as input data to the neural network. In comparing the feature values extracted by DWT for each image, the horizontal and vertical low frequencies showed similar patterns, but the patterns were different in the horizontal and vertical high frequency and diagonal high frequency regions. In particular, the signal value was large in the T1 and T2 weighted images of MRI. Neural network learning results for fitting degree analysis were as follows.

1. T1-weighted MRI and simultaneous MR-PET image fitting degree: Regression (R) values were found to be Training 0.984, Validation 0.844, and Testing 0.886.
2. Dementia-PET image and Simultaneous MR-PET Image fitting degree: R values were found to be Training 0.970, Validation 0.803, and Testing 0.828.
3. T2-weighted MRI and concurrent MR-PET image fitting degree: R values were found to be Training 0.999, Validation 0.908, and Testing 0.766.
4. Brain tumor-PET image and Simultaneous MR-PET image fitting degree: R values were found to be Training 0.999, Validation 0.983, and Testing 0.876.

An R value closer to 1 indicates more similarity. Therefore, each image fused in the simultaneous MR-PET images verified in this study was found to be similar. Ongoing study of images acquired with pulse sequences other than the weighted images in the MRI is needed. These studies may establish a useful protocol for the acquisition of simultaneous MR-PET images.

Keywords: Simultaneous MR-PET, Medical image registration, Feature extraction, Artificial intelligence, Neural networks

[1]*GilJae Lee*
Business Promotion Agency, Chungbuk Technopark (28116)40, Yeongudanji-ro, Cheongju-si, Chungcheongbuk-do, Korea

[1†]*Hwunjae Lee*
Department of Radiology, College of Medicine (03722)Yonsei University, 50-1, Yonsei-ro, Seodaemoon-gu, Seoul, Korea
YUHS-KRIBB Medical Convergence Research Institute, College of Medicine, Yonsei University, Seoul, Korea

[2*]*Gyehwan Jin* (✉) ***corresponding author***
Dept. of Radiology, Nambu University (62271)Deptartment of Radiology, Nambu University 23 Chumdan Jungang-ro, Gwangsan-gu, Gwangju, Korea

I. Introduction

The discovery of x-rays provided a way to see inside the human body for the first time in history and has been an opportunity for the

development of modern medicine [1]. In the late 20th century, advanced imaging techniques such as computed tomography (CT), magnetic resonance imaging (MRI), and positron emission tomography (PET) were developed by grafting computer technology to medical imaging equipment. These medical imaging devices enable evaluation of the anatomy and physiological characteristics of the human body and can express these characteristics in 3D high resolution [2]. The simultaneous MR-PET examination can obtain images of higher soft tissue contrast while exposing the patient to less radiation compared with the PET-CT examination. The reason is that 70% of radiation exposure in PET/CT scans is from CT, and MRI has higher soft tissue contrast than CT [3]. Therefore, simultaneous MR-PET testing is advantageous for testing patients of reproductive age, children, and pregnant women [3]. Simultaneous MR-PET acquires an image in one session and completely registers anatomical and functional information. In contrast, sequential PET-MRI may cause resampling and registration errors between the PET scan and the MRI scan by sequentially performing two scans. In addition, the sequential PET-MRI examination increases the examination time, causing inconvenience to the patient. From a technical point of view, patient motion is a major problem with whole-body PET scans and affects image quality and quantification [3]. Simultaneous MR-PET scans are integrated into the modeling and PET reconstruction process to provide accurate motion measurements that can produce motion-free PET images [3].

In this paper, we evaluated whether the fusion image acquired by simultaneous MR-PET was properly mapped (fitting degree) to the characteristics of the PET image and the characteristics of the MRI. In the evaluation, after segmenting the experimental image, features were extracted by DWT, and the extracted feature values were used as input signals to the neural network to be evaluated by machine learning.

II. Materials and Methods

1. Simultaneous MR-PET images

Simultaneous MR-PET is a method that can simultaneously perform PET using radiopharmaceuticals that emit positrons and MRI using superconducting magnets and radio high frequency [7]. Simultaneous MR-PET is a fusion molecular imaging system that combines PET that shows ultra-sensitive molecular images and MRI capable of high-resolution functional imaging. It has the advantages of improved diagnostic accuracy compared with xxxx, aids in developing new imaging biomarkers and new drugs, reduced radiation exposure, and improved patient convenience [7]. Compared with PET-CT, PET-MRI exposes patients to less radiation (up to 70% of the dose received from PET-CT scans is due to CT) and has a higher contrast for soft tissue [5]. Since simultaneous MR-PET is an all-in-one device, it acquires two examinations at the same time, reducing the examination time by almost half compared with the device that acquires PET and MRI in sequence [7]. Therefore, the accuracy of the examination, patient convenience, and the profitability of the equipment are increased. For example, due to simultaneous acquisition, errors due to movement are minimized, thereby increasing the accuracy of diagnosis around a moving bowel and a bladder filled with urine. In simultaneous MR-PET, measurements can be performed in one single session, but separate scanners have to adjust the two examinations, which further affects the overall examination time and patient comfort [7]. Simultaneous MR-PET can provide complete registration with anatomical and functional information, but sequential PET-MRI can cause errors due to resampling and registration between PET and MRI images. Simultaneous MRI scans are integrated into the modeling and PET reconstruction process to provide accurate motion measurements that can produce motion-free PET images [7]. PET also provides quantitative functional information as long as certain data modifications, such as attenuation and scattering of γ photons in patient tissue, are applied correctly. CT provides contrast information for X-ray absorption based on the electron density of the tissue, whereas MRI provides contrast information for the proton density of tissue [8]. Other strategies for converting proton density to electron density in specific cases of brain PET have been studied [9].

The combination of PET and MRI requires significant advances in the software that supports the

measurement of signals such as the influence of the magnetic field by the superconducting magnet of the MRI, attenuation and motion compensation, and design errors in the new RF coil on the PET amplification device [7].

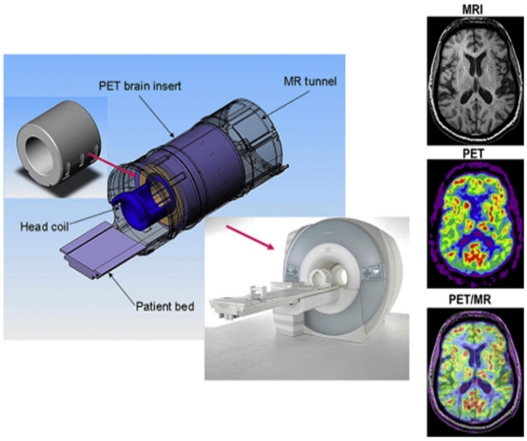

Figure 1. Simultaneous MR-PET diagram and images[4]

2. Feature extraction of simultaneous MR-PET images by discrete wavelet transform (DWT)

Wavelet transforms can construct a model of a signal, system, or process into a specific set of signals [10]. This special signal is called a wavelet, and it is expressed as an arbitrary waveform through a localized small wavelet as a pattern and is transformed, enlarged, or reduced. The characteristic of time-frequency analysis by wavelet transformation is that the time resolution is high in the high-frequency domain and the frequency resolution is high in the low-frequency domain [10]. The two-dimensional wavelet decomposition algorithm of the image works similarly to the one-dimensional case. The two-dimensional wavelet and scaling function are obtained by taking the tensor product and scaling function of the one-dimensional wavelet.

This kind of two-dimensional DWT decomposes the approximation coefficient at level j into four components, the approximation at level j + 1 and the detail in three directions (horizontal, vertical, and diagonal) [10]. [Figure 2] explains the decomposition step [11].

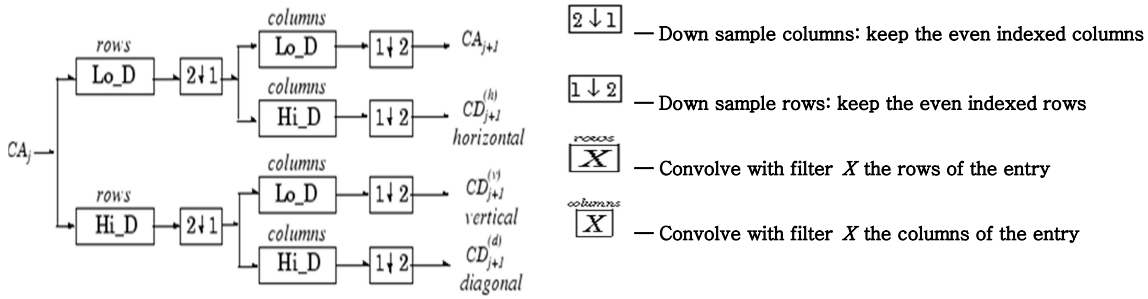

Figure 2. Decomposition step of the image by DWT[11]

3. Self-organizing maps (SOM)

The feature mapping of the structure of a self-organizing neural network is the transformation of input patterns of any dimension into outputs of neurons composed of a one-dimensional or two-dimensional array. The neural network that performs these ideas is called a feature map [12]. In addition to dimensional reduction, feature maps also have features that preserve topology. That is, input patterns that are close to each other activate output units that are close to each other in the feature map. This is also an important feature of feature maps found in the cerebral cortex of developed animals [12]. SOM is generally composed of a one-dimensional or two-dimensional array of units, and each unit is connected to all n input nodes. If the n-dimensional vector of the unit in (i, j) is w_{ij}, each neuron calculates the Euclidean distance between the input vector and the stored connection strength vector w_{ij} [12][13].

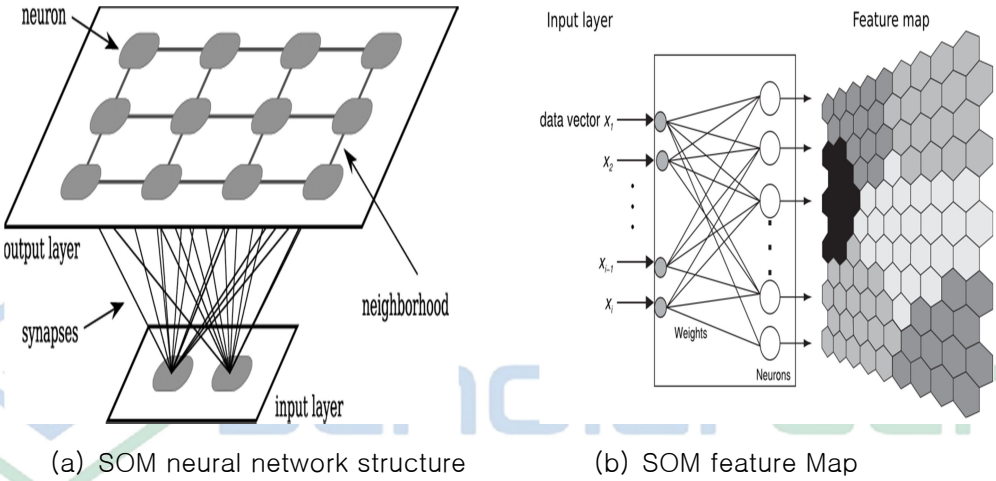

Figure 3. Self-Organizing Maps (SOM)[12][13]

III. Experimental Results and Discussion

The experiment was performed following the experimental concept diagram in [Figure 4]. The fitting degree of the MR and PET images of the simultaneous MR-PET image of (2) acquired with the equipment (1) in [Figure 4] was analyzed. In step (3), each image (MRI, PET, simultaneous MR-PET image) for the experiment was subjected to DWT. Low-frequency coefficient matrix 6 X 16 feature parameters were extracted with the 3-step DWT. The extracted parameters were input to the SOM neural network configured in (4) and the result was obtained in (5).

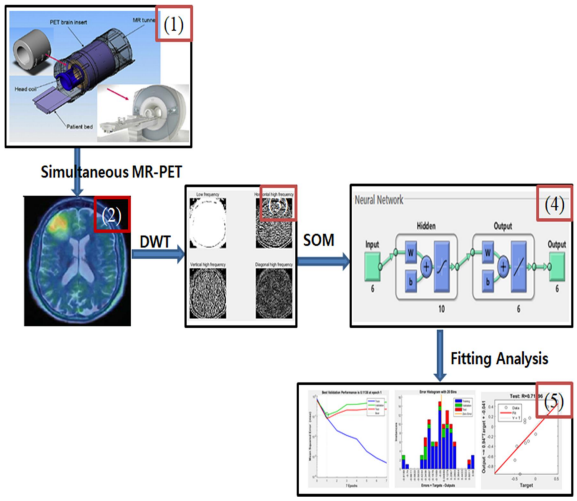

Figure 4. Experimental procedure

1. Image acquisition and preprocessing

Figure 5 and Figure 6 show the medical images used in the experiment. The experimental image was adjusted to 256 X 256 pixels, and the image shape was pre-processed in the form of a bit map (*.bpm).

To extract the features of the experimental image, we implemented and executed the DWT program using Matlab R2015. The experiment was conducted with the SOM neural network using the extracted features as input.

A. T1-weighted MRI and Dementia PET fusion image

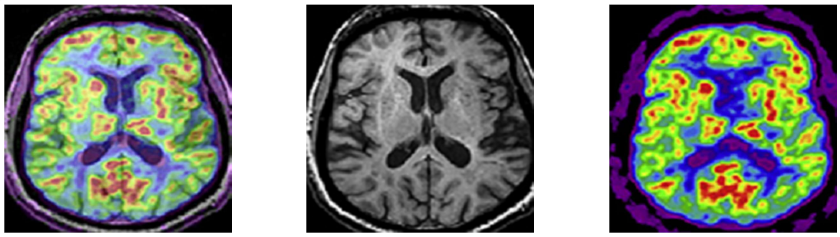

(a) Fusion Image (b) T1-weighted MRI (c) Dementia PET Image

Figure 5. T1-weighted MRI and Dementia PET fusion images

B. T2-weighted MRI and brain tumor PET fusion image

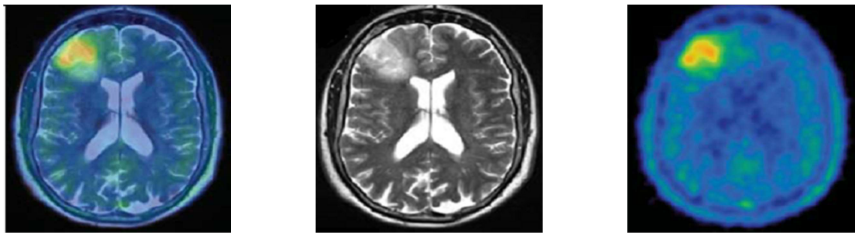

(a) Fusion Image (b) T2-wighted MRI Brain tumor PET Image

Figure 6. T2-weighted MRI and brain tumor PET fusion images

2. DWT

Matlab M-Programing was performed for DWT. The experimental images were performed by pre-processing the six images in Figures 5 and 6 into 256 X 256 pixels and then segmenting the disease area.

A. T1-weighted MRI (T1WI) and Dementia PET fusion image

[Table 1] shows the 6 X 16 matrix feature extraction values obtained as a result of 3-step DWT after the segmentation of a simultaneous MR-PET (T1WI and Dementia PET fusion image) image.

Table 1. Feature extraction results of Simultaneous MR-PET (T1WI and Dementia PET fusion image)

Features of T1-weighted MRI and Dementia PET fusion image																
A4H	-0.50	-0.50	-0.50	-0.49	-0.48	-0.48	-0.18	0.15	0.29	0.35	0.40	0.42	0.47	0.49	0.50	0.50
A4V	-0.50	-0.50	-0.50	-0.49	-0.44	-0.11	0.13	0.25	0.35	0.40	0.48	0.48	0.47	0.50	0.38	0.43
H4V	-0.50	-0.50	-0.48	-0.40	-0.41	0.11	0.50	-0.07	-0.16	-0.39	-0.36	-0.44	-0.43	-0.44	-0.42	-0.45
V4H	-0.50	-0.50	-0.49	-0.25	0.50	0.01	-0.17	-0.29	-0.41	-0.42	-0.28	-0.22	-0.47	-0.37	-0.30	-0.22
D4H	-0.50	-0.50	-0.49	-0.40	-0.33	0.50	0.38	0.00	0.04	-0.40	-0.28	-0.30	-0.30	-0.41	-0.37	-0.42
D4V	-0.50	-0.50	-0.48	0.03	0.50	0.10	0.07	0.07	-0.25	-0.09	0.16	0.02	-0.44	-0.24	-0.04	0.10

1) Feature extraction of T1WI

[Table 2] shows the 6 X 16 matrix feature extraction values obtained as a result of 3-step DWT after the segmentation of T1WI.

Table 2. Feature extraction results of T1-weighted MRI

Features of T1-weighted MRI																
A4H	-0.50	-0.48	-0.28	-0.18	-0.10	-0.26	-0.12	0.06	0.14	0.14	0.24	0.29	0.39	0.47	0.50	0.34
A4V	-0.50	-0.49	-0.47	-0.45	-0.24	-0.08	0.06	0.25	0.34	0.47	0.50	0.27	0.40	0.42	0.33	0.42
H4V	-0.50	0.26	0.33	0.35	0.50	0.29	-0.05	-0.28	-0.13	-0.07	-0.09	-0.09	-0.17	-0.23	-0.09	0.17
V4H	-0.50	-0.19	0.05	0.26	0.34	0.37	0.03	0.43	-0.16	0.08	0.50	0.42	0.26	0.42	0.14	0.43
D4H	-0.50	-0.10	0.22	0.34	0.41	0.06	0.50	0.38	0.09	0.15	0.35	-0.09	-0.09	-0.14	0.27	0.20
D4V	-0.50	-0.24	0.11	0.08	0.07	0.25	-0.16	0.05	-0.30	0.11	0.12	0.50	0.07	-0.13	-0.10	0.22

Each parameter (A4H, A4V, V4H, H4V, D4H, D4V) in [Table 1] and [Table 2] containing the feature extraction values obtained by DWT is shown as a graph. [Figure 7] shows graphs of A4H (horizontal low-frequency characteristics) and A4V (vertical low-frequency characteristics) in [Table 1] and [Table 2]. The results show that the characteristics of the vertical and horizontal low-frequency regions are similar.

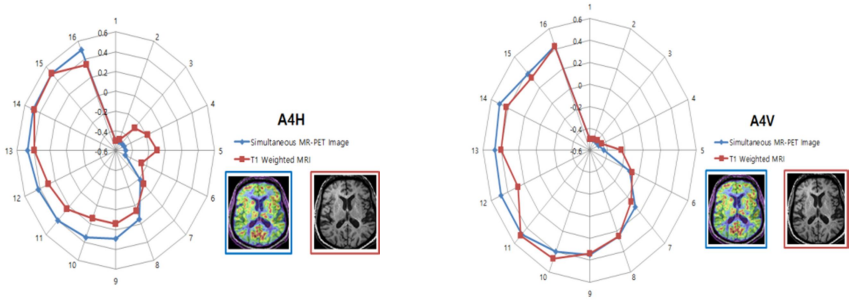

Figure 7. A4H (horizontal low frequency characteristics) and A4V (vertical low-frequency characteristics) graph in [Table 1] and [Table 2]

[Figure 8] shows graphs of H4V (horizontal high-frequency feature) and V4H (vertical high-frequency feature) in [Table 1] and [Table 2]. The characteristics of the vertical and horizontal high-frequency regions are different, and the results show that the T1WI image contains many high-frequency components.

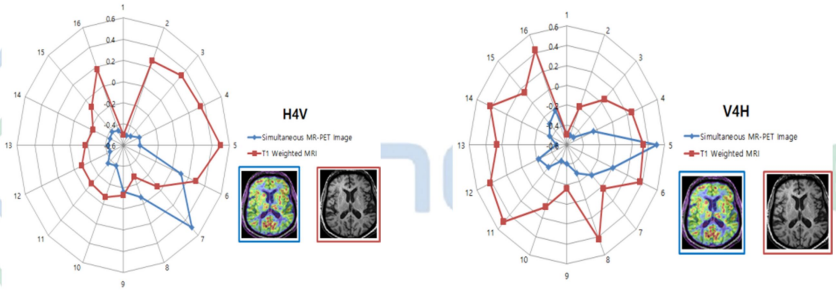

Figure 8. H4V (horizontal high frequency characteristic) and V4H (vertical high frequency characteristic) graph in [Table 1] and [Table 2]

[Figure 9] shows graphs of D4H (diagonal high-frequency characteristics) and D4V (diagonal low-frequency characteristics) in [Table 1] and [Table 2]. The characteristics of the frequency domain in the diagonal direction are different, and the results show that the T1WI image has many frequency components.

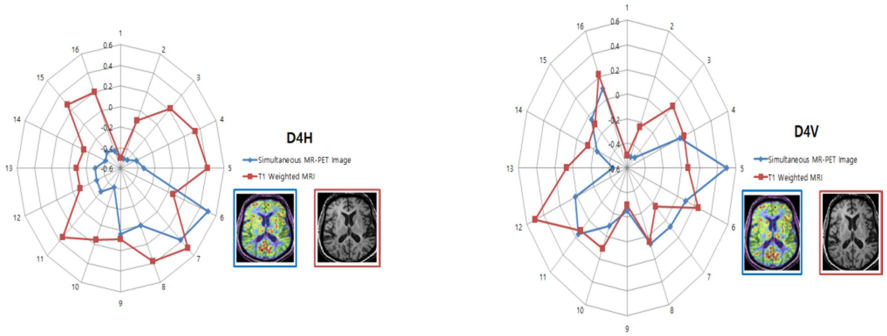

Figure 9. D4H (diagonal high frequency characteristics) and D4V (diagonal low frequency characteristic) graph in [Table 1] and [Table 2]

2) Feature extraction of Dementia PET image

[Table 3] shows the 6 X 16 matrix feature extraction values obtained as a result of 3-step DWT after segmentation of the Dementia-PET image.

Table 3. Feature extraction results of Dementia PET image

Features of Dementia PET image																
A4H	-0.50	-0.50	-0.50	-0.50	-0.50	-0.50	-0.46	-0.07	0.09	0.22	0.36	0.41	0.45	0.48	0.49	0.50
A4V	-0.50	-0.50	-0.50	-0.50	-0.48	-0.21	0.08	0.22	0.32	0.40	0.47	0.50	0.48	0.50	0.26	0.44
H4V	-0.50	-0.50	-0.50	-0.50	-0.50	-0.38	0.50	0.12	0.09	-0.10	-0.42	-0.40	-0.43	-0.48	-0.43	-0.48
V4H	-0.50	-0.50	-0.50	-0.44	0.49	0.37	-0.02	-0.11	-0.24	-0.42	-0.42	-0.44	-0.39	0.50	0.21	-0.29
D4H	-0.50	-0.50	-0.50	-0.50	-0.50	-0.31	0.50	-0.09	0.17	0.04	-0.26	-0.23	-0.40	-0.48	-0.35	-0.45
D4V	-0.50	-0.50	-0.50	-0.48	0.11	0.50	0.09	0.18	-0.19	0.02	-0.24	-0.38	-0.21	0.26	0.07	-0.06

[Figure 10] shows graphs of A4H (horizontal low frequency characteristics) and A4V (vertical low frequency characteristics) in [Table 1] and [Table 3]. The results show that the characteristics of the vertical and horizontal low frequency regions are similar.

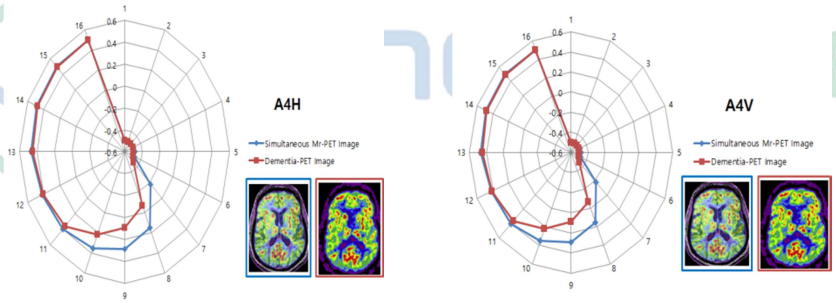

Figure 10. A4H (horizontal low frequency characteristics) and A4V (vertical low-frequency characteristics) graph in [Table 1] and [Table 3]

[Figure 11] is a graph showing H4V (horizontal high frequency characteristics) and V4H (vertical high frequency characteristics) in [Table 1] and [Table 3]. The results show that the characteristics of the vertical and horizontal high-frequency regions are different and that the Dementia-PET image has more high-frequency components.

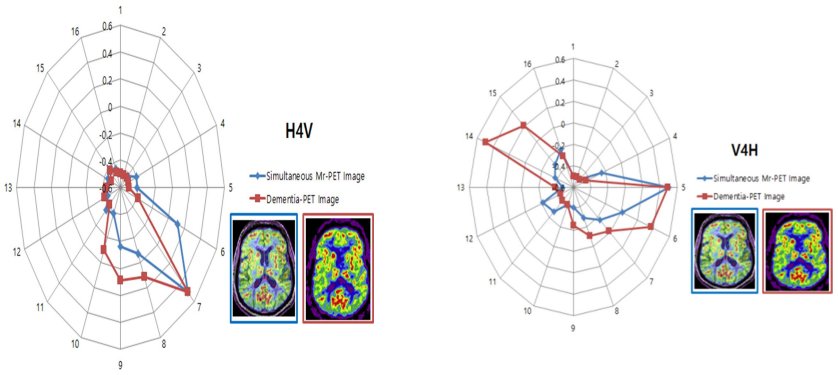

Figure 11. H4V (horizontal high frequency characteristic) and V4H (vertical high frequency characteristic) graph in [Table 1] and [Table 3]

[Figure 12] shows graphs of D4H (diagonal high-frequency characteristics) and D4V (diagonal low-frequency characteristics) in [Table 1] and [Table 3]. The results show that the characteristics of the diagonal high-frequency region are similar.

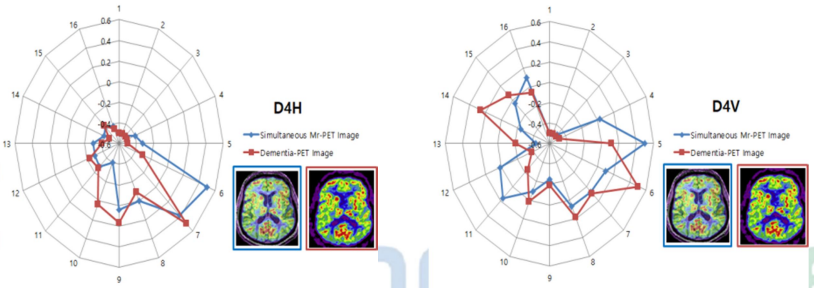

Figure 12. D4H (diagonal high frequency characteristics) and D4V (diagonal low frequency characteristic) graph in [Table 1] and [Table 3]

B. T2-weighted MRI (T2WI) and brain tumor PET fusion image

[Table 4] shows the 6 X 16 matrix feature extraction values obtained as a result of 3-step DWT after segmentation of simultaneous MR-PET (T2WI and Brain tumor-PET fusion image) images.

Table 4. Feature extraction results of Simultaneous MR-PET (T2WI and brain tumor PET fusion image) image

Features of T2-weighted MRI and brain tumor PET fusion image																
A4H	-0.50	-0.50	-0.50	-0.50	-0.50	-0.50	-0.47	-0.29	-0.38	-0.10	0.11	0.34	0.50	0.44	0.17	-0.29
A4V	-0.50	-0.50	-0.50	-0.49	-0.45	-0.37	-0.02	0.28	0.44	0.50	0.38	0.10	-0.36	-0.38	-0.42	-0.46
H4V	-0.50	-0.50	-0.48	-0.50	-0.50	-0.48	0.22	-0.04	0.09	-0.23	-0.33	-0.38	-0.37	0.00	0.50	0.36
V4H	-0.50	-0.50	-0.50	-0.28	0.26	0.08	0.15	-0.14	-0.05	0.12	0.50	0.45	0.10	0.17	-0.20	-0.33
D4H	-0.50	-0.50	-0.43	-0.48	-0.50	-0.47	0.41	0.45	0.28	-0.04	0.28	-0.04	-0.12	0.38	0.50	0.50
D4V	-0.50	-0.50	-0.50	-0.16	0.02	0.48	0.11	-0.14	-0.01	0.35	0.50	0.36	0.14	0.37	-0.32	-0.24

1) Feature extraction of T2WI

[Table 5] shows the 6 X 16 matrix feature extraction values obtained as a result of 3-step DWT after

segmentation of T2WI.

Table 5. Feature extraction results of T2WI

Features of T2-weighted MRI																
A4H	-0.50	-0.49	-0.42	-0.38	-0.45	-0.35	-0.24	-0.10	0.06	0.08	0.24	0.41	0.50	0.29	0.09	-0.01
A4V	-0.50	-0.50	-0.50	-0.47	-0.29	-0.08	0.05	0.29	0.38	0.50	0.37	0.24	-0.24	-0.13	-0.26	-0.30
H4V	-0.50	-0.29	0.06	-0.30	-0.08	0.50	0.44	0.14	-0.16	-0.25	-0.28	-0.42	-0.17	-0.12	0.06	-0.03
V4H	-0.50	-0.50	-0.50	0.06	0.50	0.08	-0.19	-0.28	-0.18	0.14	-0.01	0.25	0.26	0.17	0.01	-0.37
D4H	-0.50	-0.43	-0.38	-0.23	-0.06	-0.03	0.50	0.25	-0.06	-0.08	-0.12	-0.43	-0.18	-0.22	-0.18	0.12
D4V	-0.50	-0.50	-0.49	-0.26	-0.10	0.50	0.04	0.27	0.26	0.37	0.26	0.02	0.00	0.13	0.17	0.04

[Figure 13] shows graphs of A4H (horizontal low frequency characteristics) and A4V (vertical low frequency characteristics) in [Table 4] and [Table 5]. The results show that the characteristics of the low frequency region are similar.

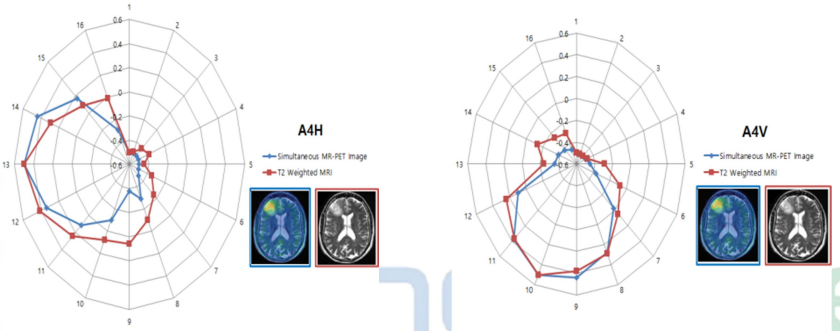

Figure 13. A4H (horizontal low frequency characteristics) and A4V (vertical low-frequency characteristics) graph in [Table 4] and [Table 5]

[Figure 14] shows graphs of H4V (horizontal high frequency characteristics) and V4H (vertical high frequency characteristics) in [Table 4] and [Table 5]. The results show that the characteristics of the high-frequency region are less than that of the low-frequency region, but are similar.

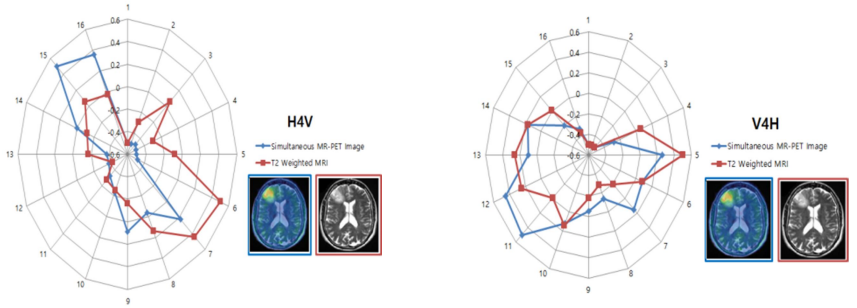

Figure 14. H4V (horizontal high frequency characteristic) and V4H (vertical high frequency characteristic) graph in [Table 4] and [Table 5]

[Figure 15] shows graphs of D4H (diagonal high-frequency characteristics) and D4V (diagonal low-frequency characteristics) in [Table 4] and [Table 5]. The results show that the characteristics of the

diagonal high-frequency region are less than that of the low-frequency region, but are similar.

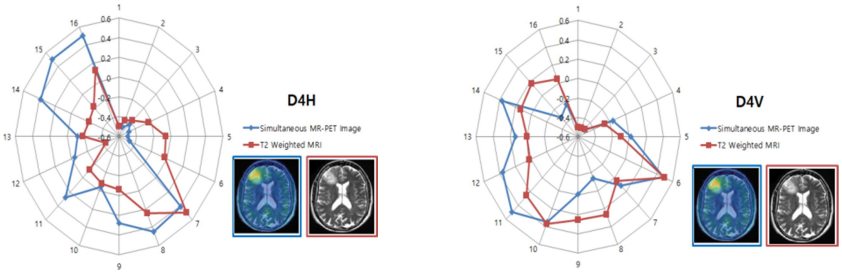

Figure 15. D4H (diagonal high frequency characteristics) and D4V (diagonal low frequency characteristic) graph in [Table 4] and [Table 5]

2) Feature extraction of brain tumor PET image

[Table 6] shows the 6 X 16 matrix feature extraction values obtained as a result of 3-step DWT after segmentation of a brain tumor-PET image.

Table 6. Feature extraction results of brain tumor PET image

Features of brain tumor PET image																
A4H	-0.50	-0.50	-0.50	-0.50	-0.50	-0.50	-0.50	-0.50	-0.47	-0.10	0.30	0.50	0.43	0.41	0.30	-0.43
A4V	-0.50	-0.50	-0.50	-0.50	-0.50	-0.47	0.03	0.32	0.42	0.50	0.00	-0.50	-0.50	-0.50	-0.50	-0.50
H4V	-0.50	-0.50	-0.50	-0.50	-0.50	-0.50	-0.50	-0.41	0.29	0.26	0.04	-0.36	-0.41	0.20	0.50	-0.32
V4H	-0.50	-0.50	-0.50	-0.50	-0.41	-0.18	-0.20	-0.33	-0.38	0.50	0.26	-0.49	-0.50	-0.50	-0.50	-0.50
D4H	-0.50	-0.50	-0.50	-0.50	-0.50	-0.50	-0.50	-0.45	-0.28	0.50	0.14	-0.26	-0.46	0.24	0.19	-0.42
D4V	-0.50	-0.50	-0.50	-0.50	-0.45	0.33	0.50	0.03	-0.14	0.39	-0.17	-0.48	-0.50	-0.50	-0.50	-0.50

[Figure 16] shows graphs of A4H (horizontal low frequency features) and A4V (vertical low frequency features) in [Table 4] and [Table 6]. The results show that the characteristics of the low frequency region are similar.

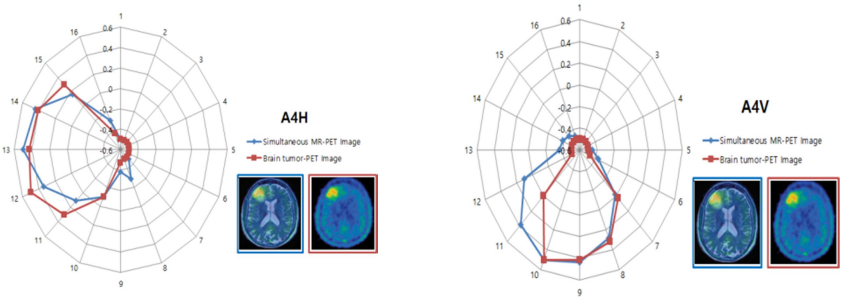

Figure 16. A4H (horizontal low frequency characteristics) and A4V (vertical low-frequency characteristics) graph in [Table 4] and [Table 6]

[Figure 17] is a graph showing H4V (horizontal high frequency feature) in [Table 4] and [Table 6] and V4H (vertical high frequency feature) in [Table 4] and [Table 6]. The results show that the characteristics of the horizontal and vertical high frequency regions are different.

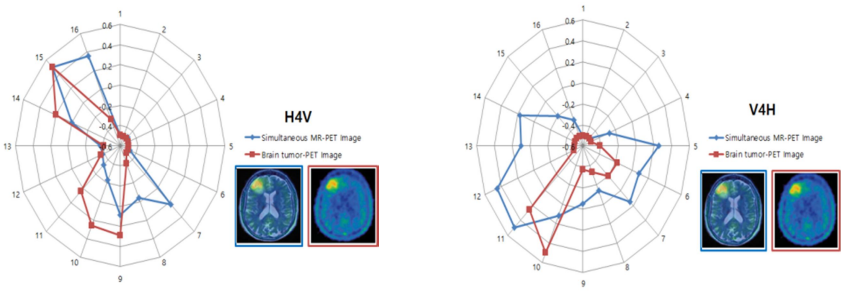

Figure 17. H4V (horizontal high frequency characteristic) and V4H (vertical high frequency characteristic) graph in [Table 4] and [Table 6]

[Figure 18] is a graph showing D4H (diagonal high-frequency characteristics) and D4V (diagonal low-frequency characteristics) in [Table 4] and [Table 6]. The results show that the characteristics of the diagonal high-frequency regions are different.

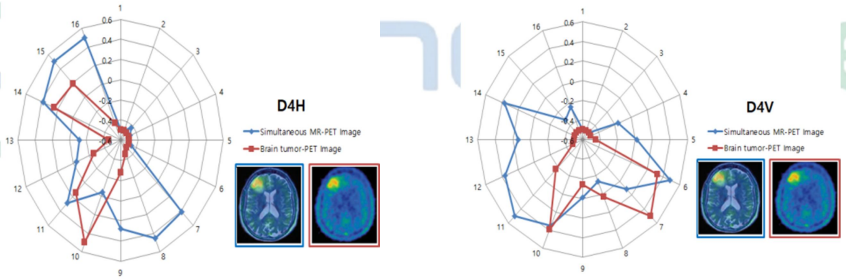

Figure 18. D4H (diagonal high frequency characteristics) and D4V (diagonal low frequency characteristic) graph in [Table 4] and [Table 6]

3. Neural network machine learning

[Figure 19] is a model diagram of a neural network for this experiment. The input variables are sequentially input 16 times with 6 extracted feature values, and learned, 10 hidden layers, 6 output layers, and 6 output values.

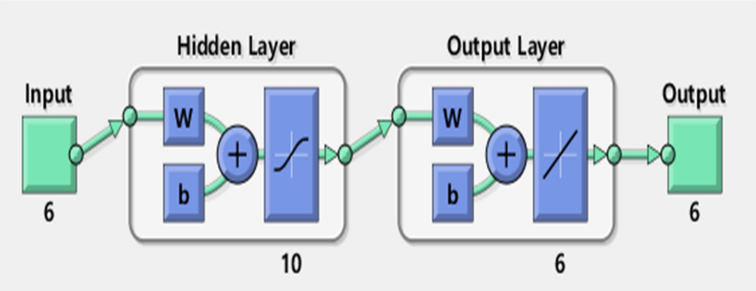

Figure 19. Neural Networks

The Levenberg-Marquardt algorithm (LMA or LM), also known as the damped least squares (DLS) method in mathematics and computing, is used to solve nonlinear least-squares problems [14][15]. This minimization problem especially arises in the least-squares curve fitting. This algorithm usually uses more memory but takes less time. When the generalization improvement stops as the mean squared error of the validation sample increases, learning is automatically stopped. In learning, the mean squared error is the mean squared difference between the output and the target [9]. A lower value is better, and 0 means no error. The regression R-value measures the correlation between the output and the target. An R-value of 1 means a close relationship, while an R-value of 0 means a random relationship [14][15].

A. T1WI and Dementia PET fusion image

1) Fitting degree of T1WI and simultaneous MR-PET images

[Figure 19] The T1WI feature value in [Table 2] was input as the input data of the neural network; for target data, the simultaneous MR-PET (T1WI and Dementia PET fusion image) feature values in [Table 1] were input. During learning, the mean squared error (MSE) is the mean squared difference between the output and the target [14]. A smaller value indicates fewer errors. The regression R-value is a measure of the correlation between the output and the target. If the R-value is close to 1, the relationship is close [14][15]. [Table 7] shows that the R-value is close to 1 for all of the training, validation, and testing, indicating that the T1WI and simultaneous MR-PET images are well fit.

Table 7. Result of neural network machine learning (T1-weighted MRI and simultaneous MR-PET images)

	Sample	MSE	R
Training	12	5.00E-03	9.9999E-01
Validation	2	2.96E-02	8.4422E-01
Testing	2	3.70E-02	8.85649E-01

[Figure 20] is a graph showing the regression.

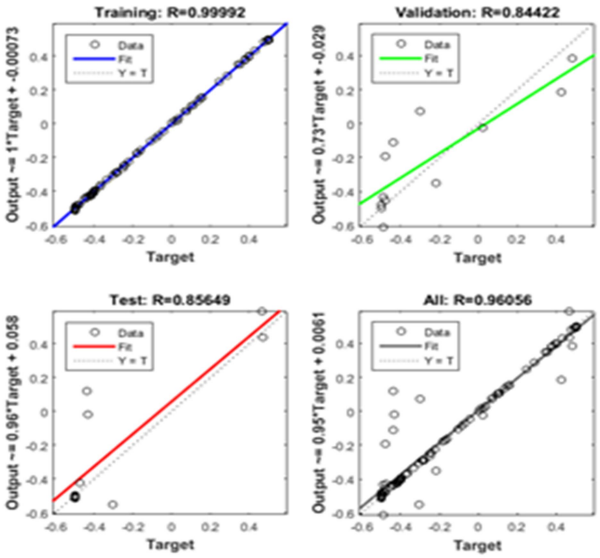

Figure 20. Regression graph (T1-weighted MRI and simultaneous MR-PET images)

2) Fitting degree of dementia PET image and simultaneous MR-PET images

[Figure 19] For the input data of the neural network, the characteristic values of the Dementia-PET image in [Table 3] were input; for the target data, the simultaneous MR-PET (T1WI and Dementia PET fusion image) feature values in [Table 1] were input. [Table 8] shows that the R-value is close to 1 for all of the training, validation, and testing, indicating that the Dementia-PET image and the simultaneous MR-PET image are fitting.

Table 8. Result of neural network machine learning (dementia PET image and simultaneous MR-PET images)

	Sample	MSE	R
Training	12	5.91E-03	9.7027E-01
Validation	2	2.89E-02	8.0298E-01
Testing	2	5.15E-02	8.2837E-01

[Figure 21] is a graph showing regression.

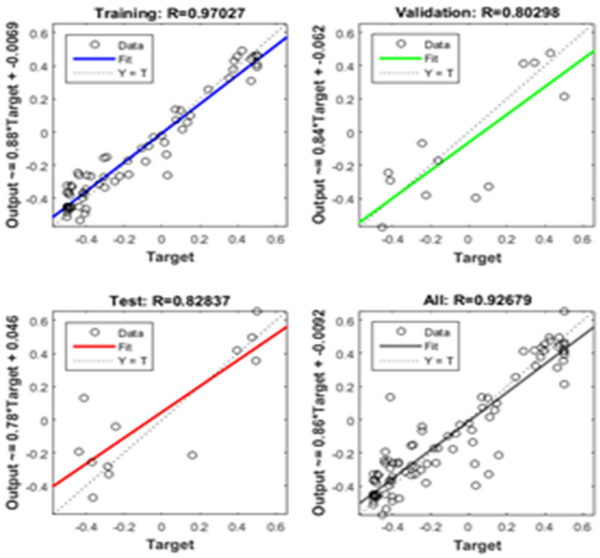

Figure 21. Regression graph (dementia PET image and simultaneous MR-PET images)

B. T2WI and brain tumor PET fusion image

1) Fitting degree of T2WI and simultaneous MR-PET images

[Figure 19] For the input data of the neural network, the T2WI feature values in [Table 5] were input; for the target data, the simultaneous MR-PET (T2WI and Brain tumor-PET fusion image) feature values in [Table 4] were input. [Table 9] shows that the R-value is close to 1 in all of the training, validation, and testing, indicating that the T2WI and simultaneous MR-PET images are well fit.

Table 9. Result of neural networks learning (T2-weighted MRI and simultaneous MR-PET images)

	Sample	MSE	R
Training	12	2.49E-03	9.9962E-01
Validation	2	1.92E-02	9.0777E-01
Testing	2	1.57E-01	7.6643E-01

[Figure 22] is a graph showing regression.

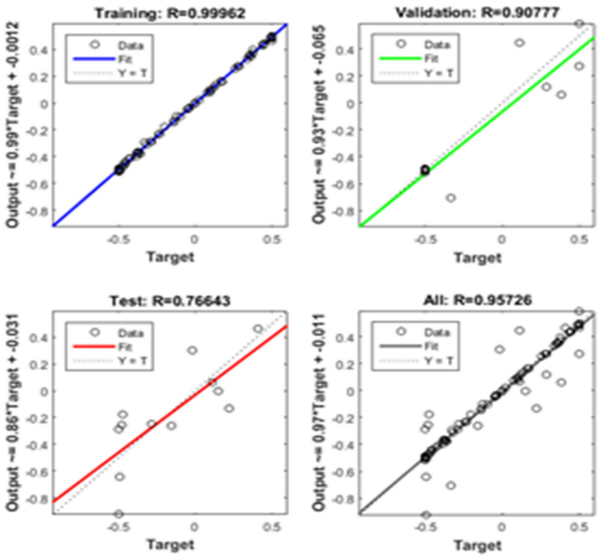

Figure 22. Regression graph (T2-weighted MRI and simultaneous MR-PET images)

2) Fitting degree of brain tumor PET image and simultaneous MR-PET images

[Figure 19] The Brain tumor-PET characteristic values in [Table 6] were input as input data of the neural networks. As target data, the simultaneous MR-PET (T2WI and Brain tumor-PET fusion image) feature values in [Table 4] were input. [Table 10] shows that the R-value is close to 1 for both training, validation, and testing, indicating that the brain tumor-PET image and the simultaneous MR-PET image are well fit.

Table 10. Result of neural networks machine learning (brain tumor PET image and simultaneous MR-PET images)

	Sample	MSE	R
Training	12	2.49E-03	9.9969E-01
Validation	2	1.92E-02	9.8251E-01
Testing	2	1.57E-01	8.7602E-01

[Figure 23] is a graph showing regression.

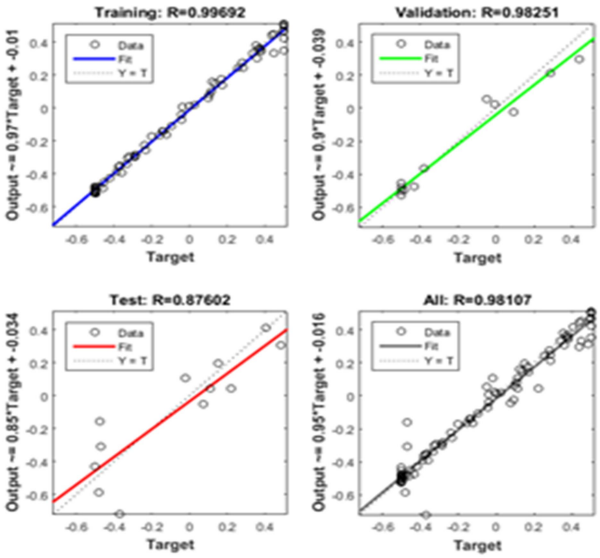

Figure 23. Regression graph (brain tumor PET image and simultaneous MR-PET images)

IV. Conclusion

With the advancement of science and technology, the era of the 4th industrial revolution is coming. In the medical field, the 4th industrial revolution has unified patient diagnosis and treatment, and the medical environment is rapidly changing from standardized evidence-based medicine to personalized precision medicine. The center of change in the medical environment is artificial intelligence (AI) technology. AI technology will be used in the entire 'before, middle, and after' process of diagnostic imaging equipment, such as CT, MRI, PET/CT, and simultaneous MR-PET, thereby providing a foundation for providing faster and more precise medical images. Simultaneous MR-PET, the state-of-the-art imaging device, significantly reduces radiation exposure (70% or more) compared with PET-CT, while the contrast of soft tissues is superior to that of PET-CT. If images are scanned with sequential MR-PET equipment, a separate process of registration after saving each acquired image is required, and the possibility of errors cannot be ruled out. Simultaneous MR-PET is a device that simultaneously acquires and stores MR images and PET images in one session. In this paper, we tested and evaluated neural networks to ascertain how well the fusion images acquired by simultaneous MR-PET were mapped (fit degree) in the fused image of MRI and PET features. After pre-processing the experimental images at 256 X 256 pixels, the disease-like regions (regions with strong signals) were segmented with a threshold of 127. The segmented image was transformed into a 3-step 2D DWT to extract 6 X 16 feature values for each image. When comparing the extracted feature values for each image, we found that the low-frequency regions in the horizontal and vertical directions showed similar patterns, but the patterns were different in the high-frequency regions in the horizontal and vertical directions,

as well as the high-frequency regions in the diagonal direction. In particular, the signal values were large in the MRI T1 and T2 images.

The following results were obtained through neural network machine learning to analyze the degree of fitting.

1. Fitting degree of T1WI and simultaneous MR-PET images:

The regression (R) values were 0.984 for Training, 0.844 for Validation, and 0.886 for Testing.

2. Fitting degree of Dementia-PET and simultaneous MR-PET images:

The R values were 0.970 for Training, 0.803 for Validation, and 0.828 for Testing.

3. Fitting degree of T2-weighted MRI and simultaneous MR-PET images:

The R value s were 0.999 for Training, 0.908 for Validation, and 0.766 for Testing.

4. Fitting degree of Brain tumor–PET and simultaneous MR-PET images:

The R values were 0.999 for Training, 0.983 for Validation, and 0.876 for Testing.

An R value closer to 1 is more appropriate; therefore, each image fused in the simultaneous MR-PET image verified in this study was suitable. However, it is necessary to continue research on images acquired with pulse sequences other than emphasis images in MRI images. These studies may help establish a useful protocol for the process of acquiring simultaneous MR-PET images.

Competing interests

The authors declare that there is no conflict of interest regarding the publication of this paper

[Acknowledgments]

This study was supported by the National Research Foundation of Korea (NRF) grant funded by the Korean government (MEST) **(NRF-2020R1I1A1A01060851)** and supported (in part) by research funds from Nambu University, 2020.

[References]

[1] Peter K. Spiegel(1995), “The First Clinical X-Ray Made in America-100 Years”, AJR, Vol. 164, PP. 241~243.

[2] G. Choi S, B. Lee(2014), “Application and Prospects of Molecular Imaging”, *Journal of the Korean Society of Radiology,* Vol. 8, No. 3, PP. 123–136.

[3] Martin S Judenhofer, Hans F Wehrl, Danny F Newport, Ciprian Catana, Stefan B Siegel, Markus Becker, et al(2008), “Simultaneous PET-MRI: a new approach for functional and morphological imaging”, *Natural Medicine,* Vol. 14, PP. 459-465.

[4] Heinz-Peter W. Schlemmer, Bernd J. Pichler, Matthias Schmand, et Al, “Simultaneous MR/PET Imaging of the Human Brain”, Radiology, Volume 248, Number 3, September 2008.

[5] Yoon, Seok-Joo, Kim, Gwang-Jun, Jang, Chang-Soo(2012), “Classification of ECG arrhythmia using Discrete Cosine Transform, Discrete Wavelet Transform and Neural Network”, The Journal of the Korea institute of electronic communication science, Volume 7, Issue 4, PP. 727~732.

[6] Lim, Jong-Myeong, Yoo, Ji-Sang(2012), “Super-resolution Algorithm using Discrete Wavelet Transform for Single-image”, Journal of Broadcast Engineering, Volume 17,

Issue 2, PP. 344~353.

[7] Cornelia B. Brendle, Holger Schmidt, Sabrina Fleisher, et al(2013), “Simultaneously Accquired MR/PET Images Compared with Sequential MR/PET and PET/CT : Alignment Quality”, Radiology, Vol. 268, No. 1, pp. 190~199

[8] Park, Su A, Lee, Jun Hee, Kim, Wan Doo(2017), “Bio-fusion and Medical Device Industry”, Transaction of the KSME C: Technology and Innovation”, Volume 5, Issue 1, PP 23~52.

[9] Zaidi, Habib, Montandon, Marie-Louise(2006), “The New Challenges of Brain PET Imaging Technology”, Current Medical imaging, Volume 2, Number 1, pp. 3~13

[10] Han, Dong-Kyun, Rhim, Jae-Dong, Lee, Jun-Haeng(2008), “Improvement in the Quality of Ultrasonographic Images Using Wavelet Conversion and a Boundary Detection Filter”, Journal of the Korean Society of Radiology, Volume 2, Issue 1, pp. 23~29.

[11] Sang-Bock Lee(1999), “A Study on Recognition and Differential Compression of Disease Region in Medical Image”, Ph. D. Thesis, Cheongju University Press, Cheongju, Korea.

[12] _____, *“Draw a Kohonen SOM feature map?”*, Internet : tex.stackexchange.com/questions/144366/draw-a-kohonen-som-feature-map, Jan. 1, 2020. [Feb. 12, 2020]

[13] Michel Haritopoulos, Hujun Yin, Nigel M. Allinson(2002), “Image denoising using self-organizing map-based nonlinear independent component analysis”, Neural Networks, Volume 15, Issue 8-9, pp. 1085~1098.

[14] Yeochang Yoon, Sungduck Lee(2013.), “A Comparison of the Effects of Optimization Learning Rates using a Modified Learning Process for Generalized Neural Network”, The Korean Journal of Applied Statistics, Vol. 26, No. 5, PP. 847-856.

[15] Suji Lee(2016), “A Study on Recurrent Neural Network Training Methods for Sequential Data Regression”, Master's Thesis, Seoul National University Graduate School Press, Seoul.